# A new rotating annular photobioreactor with Taylor–Couette type flow for phototrophic biofilm investigations

**Chapter** · January 2017

CITATIONS
0

READS
51

**8 authors**, including:

Armelle Paule

**21** PUBLICATIONS **221** CITATIONS

SEE PROFILE

Aridane G. González

Universidad de Las Palmas de Gran Canaria

**64** PUBLICATIONS **760** CITATIONS

SEE PROFILE

Oleg S. Pokrovsky

GET CNRS, N. Laverov FCIAR RAS, and Tomsk State University

**458** PUBLICATIONS **11,219** CITATIONS

SEE PROFILE

*Chapter*

# NEW ROTATING ANNULAR PHOTOBIOREACTOR WITH TAYLOR-COUETTE TYPE FLOW FOR PHOTOTROPHIC BIOFILM INVESTIGATIONS

***Jean-Luc Rols[1,*], PhD, Armelle Paule[1,2], PhD, Margot A. Coutaud[1,3], PhD, Aridane G. Gonzalez[1,3], PhD, Oleg S. Pokrovsky[3], PhD, Jérôme Morchain[2], PhD, Joséphine Leflaive[1], PhD, and Etienne Paul[2], PhD***

[1]EcoLab - Laboratoire écologie fonctionnelle et environnement, Université de Toulouse, CNRS, INPT, UPS, Toulouse, France

[2]LISBP - Laboratoire ingénierie des systèmes biologiques et des procédés, Université de Toulouse, CNRS, INRA, INSA, Toulouse, France

[3]GET - Laboratoire géosciences environnement Toulouse, Université de Toulouse, CNRS, IRD, UPS, Toulouse, France

## ABSTRACT

The structure and function of microbial communities obtained from river phototrophic biofilms are driven by biotic and abiotic factors. An understanding of the mechanisms that mediate community structure, dynamics of biological succession and associated ecological functions can be obtained by using laboratory-scale systems operated under controlled parameters (e.g., hydrodynamics, light and nutrients). A new prototype of rotating annular photobioreactor (Taylor-Couette type flow) was designed to produce phototrophic biofilm under controlled environmental conditions. This photobioreactor has been successfully used in microbial ecotoxicology investigations (using alachlor herbicide and ionic Ag and Ag nanoparticles) and in studies on interaction of metals (Cu and Zn) with phototrophic biofilm.

**Keywords**: rotating annular photobioreactor, phototrophic biofilm, microbial community, organic and inorganic pollutants, biosorption

[*] Address correspondence to: jean-luc.rols@univ-tlse3.fr.

## RIVER PHOTOTROPHIC BIOFILMS

River phototrophic biofilms form on all lighted solid–liquid interface, such as surface of pebbles or plants that emerged from streams; these pebbles or plants display large surface area-to-water volume ratios. Phototrophic biofilms are complex assemblages of many heterotrophic micro- and meio-organisms (e.g., bacteria and protozoa) and phototrophic microorganisms (e.g., diatoms and cyanobacteria) embedded in an exopolymeric matrix. The latter, produced by the microorganisms themselves, consists mainly of polysaccharides, proteins, nucleic acids and lipids (notably phospholipids), known as extracellular polymeric substances (EPS). This matrix can provide protection to microbial communities and invertebrates from hydraulic shear forces and against the toxicity of water-borne pollutants.

Phototrophic biofilms are a crucial component of running water ecosystems because they play a major role in primary production (Buhman et al. 2012) and are at the base of trophic networks (Lear et al. 2012). These biofilms considerably contribute to the hydrological, physical and biogeochemical processes in running waters (Battin et al. 2003). Moreover, they contribute to the self-depuration processes (ecological services) of natural toxins or organic pollutants (Lyautey et al. 2003) and to metal sorption (Guibaud et al. 2009). Given their ubiquitous character, short generation time, sessile nature and rapid response to changes in environmental conditions (Lyautey et al. 2005a, Paule et al. 2009), phototrophic biofilms are widely used as bio-indicator of water quality in lotic systems. They have been qualified as ‘early warning pollution indicator’ (Sabater et al. 2007).

Development of phototrophic biofilm is associated with population succession processes, both for the algal and the bacterial compartments. Artificial substrates are colonized by early-colonising diatoms, which modify the microenvironment and promote settlement and colonisation of other communities. However, some environmental conditions favour the initial colonization of green algae (high light intensities) or of heterotrophic bacteria (low light intensities). The development of phototrophic biofilm is controlled by several physical (e.g., hydrodynamics, temperature and light), chemical (pH and nutrient availability) and biological (competition and grazing) factors. Biofilm thickening during growth and the subsequent formation of micro-gradients (pH, oxygen and nutrients) promote the formation of ecological niches. These transformations induce ecological successions of algal and bacterial populations, resulting in modifications of both microbial functions and nature of EPS.

The structure of a microbial community within a phototrophic biofilm is controlled by various allogenic (physico-chemistry of the water column) or autogenic (interactions between microbial populations and the formation of physico-chemical micro-gradients within biofilms) factors, whose relative importance varies during biofilm growth and maturation (Paule et al. 2013). Indeed, during biofilm thickening, interactions between microbial community and water column decreases whilst new ecological niches become available for microbial species brought by the flow. The consequence is the temporal successions of algal and bacterial populations (Jackson, 2003) with a trajectory closely linked to allogenic and autogenic factors during the early and late stages of biofilm growth, respectively (climax after 4 to 8 weeks depending on temperature, among other factors). During temporal modifications of the microbial structure of biofilms, some new functions emerge, such as internal mineralisation, nitrification and denitrification (Lyautey et al. 2005b).

The organization, development, structure or interactions of phototrophic biofilms are controlled by EPS matrix secreted by microorganisms. This matrix may represent up to 60% of the biofilm biomass and protects microorganisms from some disadvantages of the planktonic life (high exposure to physico-chemical factors and pollutants) and allows the creation of ecological niches favouring the multiplicity of microbial functions. The EPS play critical functions as they are involved in physical stability of biofilms and act as a physical barrier protecting the microorganisms (Flemming and Wingender, 2010). Proteins are implicated in the first steps in adhesion of microorganisms onto a surface and in the formation of a cohesive matrix, particularly amyloid fibre-type proteins (Larsen et al. 2007). Moreover, the EPS is involved in adsorption of organic/inorganic molecules from water column (via heavy metal precipitation and direct or indirect reduction) (Singh et al. 2006). Some proteins in the EPS are involved in enzymatic degradation of exogen macromolecules, allowing production of nutrients (Flemming and Wingender, 2010). The ability of phototrophic biofilms to retain water is rendered by the hydrophilic polysaccharides present in the EPS; these polysaccharides contain 98% water (Sutherland 2001), allowing the biofilms to withstand desiccation.

Understanding how phototrophic biofilms affect geochemical processes and their contribution in improving water chemical quality is important. Trace elements present in water interact with biofilms through physical, chemical or biological processes. The relative contributions of biotic and abiotic factors to trace metal retention strongly depend on the physico-chemical characteristics of the aqueous phase (pH and redox potential), availability of reactive mineral surface sites, abundance of strongly complexing organic functional groups and the microenvironments of the biofilm matrix within the biofilm. However, due to the complexity of these interrelationships and the difficulty in probing these microenvironments, distribution, speciation and local structure of metal sorption complexes present at the bulk-biofilm interface, as well as within the biofilm matrix, are poorly understood.

## ROTATING ANNULAR PHOTOBIOREACTOR (RAPB)

The best approach in understanding how the abiotic and biotic factors (alone or combined) influence the microbial community structure, its dynamics and the biological succession processes during development of phototrophic biofilm involves the use of laboratory-scale systems simulating environmental conditions under different levels of experimental control. Various large and small-scale laboratory systems designed to investigate phototrophic biofilms have been reported (e.g., Singer et al. 2006). The hydrodynamic conditions at the local level influence the composition and structure of biofilms (Besemer et al. 2007).

RAPBs have been suggested as a powerful tool in studying the effects of environmental changes on biofilm development (Neu and Lawrence 1997). The geometry of RAPBs facilitates the distribution of constant shear stress and the cultivation of biofilm under turbulent flow environments. Lawrence et al. (2000) developed a RAPB (with a liquid working volume of 0.5 L) for the cultivation of phototrophic biofilms. The main shortcomings of this RAPB are its small size, which limits the number of possible analyses and replicates, the external illumination and the growth of the biofilm on a rotating inner cylinder (subject to centrifugal forces). The main advantage is the number of RAPB used in parallel to test different factors affecting the microbial community (Paule et al. 2016).

Our laboratories (in collaboration with Arias, Toulouse, France) designed a new RAPB (Taylor-Couette type flow) prototype specifically intended to cultivate and investigate phototrophic biofilms; this prototype is adapted from a rotating annular bioreactor designed for wastewater treatment (Coufort et al. 2005). The innovations in our modified RAPB include the presence of a modular source of light within the system and the colonisation of biofilm into the stationary outer cylinder.

Our laboratory-scale prototype RAPB with Taylor-Couette type flow was first described by Paule et al. (2011). This RAPB consists of two concentric cylinders, a stationary outer cylinder made of polyvinyl chloride and a rotating inner cylinder made of poly(methyl methacrylate) (PMMA) (Figure 1 and Table 1). In particular, this prototype comprise the following:

- a modular source of light inside the system, protected by an internal watertight cylinder made of PMMA and adjusted by changing the quality and number of fluorescent tubes (1–8) and the frequency of light/dark cycles. At the centre of this cylinder, another cylinder made of PMMA is positioned to improve the distribution of light. The RAPB is illuminated by fluorescent lamps, consisting of equal number of cool daylight lamps (Osram L15w:865 Luminux, Germany) and fluora tubes (Osram L15W/77, Germany, emission in the visible red to enhance photosynthesis), with light/dark periods of 16 h/8 h. The number of neon tubes (2 or 4) is a good compromise to maintain illumination homogeneity (the fewer the lamps, the less uniform the light field is) and to prevent an increase in temperature generated by the presence of neon tubes (the RAPB is not thermostated).
- a flow generated in the annular gap (width, 18.5 mm) through the rotation of the inner cylinder modulated by different motor speeds (up to 200 rpm).

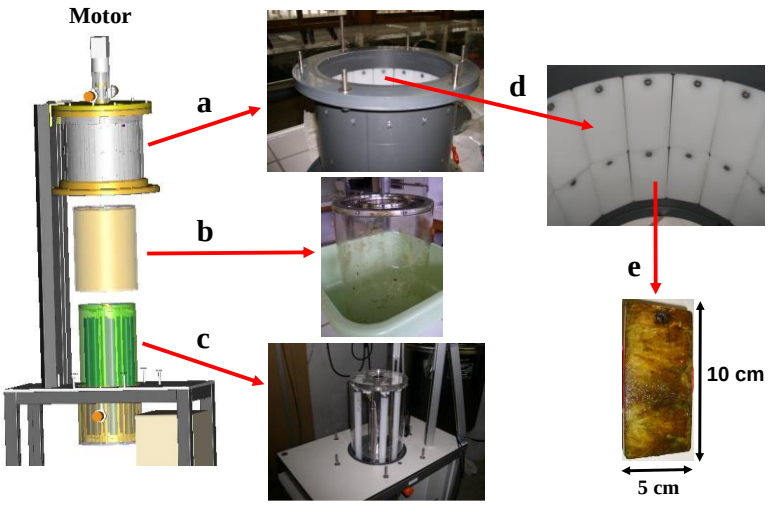


Figure 1. Setup of the rotating annular photobioreactor, a: stationary outer cylinder, b: transparent rotating inner cylinder, c: internal watertight cylinder containing light source, d: inside view of the outer cylinder with two rows of 16 removable plates, e: one plate colonized by phototrophic biofilm.

**Table 1. Characteristics of the rotating annular photobioreactor**

| | |
|---|---|
| Internal diameter of outer cylinder (mm) | 257 |
| External diameter of inner cylinder (mm) | 220 |
| Width of annular gap (mm) | 18.5 |
| Height of inner cylinder (mm) | 200 |
| Liquid working volume (L) | 5.04 |
| Surface area of one plate ($mm^2$) | 5,000 |
| Number of removable plates | 32 |
| Number of neon tubes | 1–8 |
| Rotational speed of the inner cylinder (rpm) | 0–200 |

The inside of the external cylinder supports two rows of 16 removable polyethylene plates or sampling units (l × h = 50 mm × 100 mm, 5 mm wide) for biofilm sampling. The total surface of the plates available for biofilm colonisation in the RAPB is 0.16 $m^2$. The plates were curved to avoid perturbation of the flow. To limit the occurrence of edge effects during biofilm development, we positioned the rows of plates at half the height of the photobioreactor.

To prevent unwanted biofilm formation that could attenuate light intensity and modify its spectrum, we manually cleaned the surfaces of the rotating inner and internal watertight cylinders with hydrogen peroxide (30%) followed by rinsing with demineralized water once a week. This 15-minute step is required to collect the liquid contained in the RAPB before opening, and allowed, if necessary, the collection of some plates for biofilm analyses. Once finished, new clean plates replaced the removed plates, and then the bioreactor was sealed and refilled with the collected liquid.

The physico-chemical parameters (temperature, pH and dissolved oxygen concentration) were recorded using probes (pH meter 296 WTW with electrodes sentix H 8481 HD SCHOTT, oxy 296 oxymeter WTW with a trioxmatic 701 sensor WTW) connected to multi-meters (METRAHIT) and located in an agitated cell (30 mL) positioned at the outlet valve of the RAPB.

A synthetic culture medium (tap water supplemented with $SiO_2$, $PO_4^{3-}$ and $NO_3^-$) was stored in a thermostated reservoir (150 L, model CV 150, Japy) at 4°C and used to continuously feed the RAPB (inlet throughput of 26 mL $min^{-1}$ and hydraulic residence time in the annular gap of 3.23 h) equipped with a peristaltic pump (520S/R2 220 T/MN pump with silicon tubes ID × OD = 1.6 mm × 2.4 mm).

The seeding procedure for the removable polyethylene plates in the RAPB involved two seeding phases, each was performed for 48 h in closed recirculation; the procedure was performed in an illuminated aquarium (10 L) where the inoculum was incubated. The inoculum was a re-suspension of natural phototrophic biofilms collected from various river stones, homogenised (13,500 rpm, Ultra Turrax T25) and filtered through a 250 μm and then through a 100 μm pore size filter (VWR) to remove the meiofauna. The two seeding phases were performed at a 24-hour interval; the RAPB was operated in continuous culture mode and fed with synthetic culture medium. The end of the seeding phase was defined as the start of the phototrophic biofilm culture in RAPB (day 0).

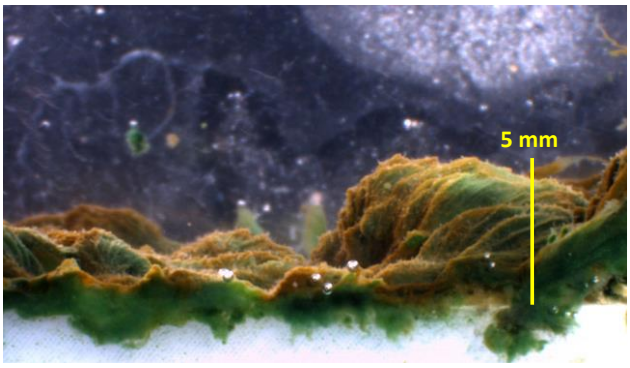


Figure 2. Sectional view of phototrophic biofilm growing on plate in the rotating annular photobioreactor after 48 days.

Figures 2 and 3 illustrate the kinetics of phototrophic biofilm production in RAPB. The RAPB was operated at a rotational speed of the inner cylinder of 80 rpm and continuously fed with a synthetic culture medium consisting of tap water supplemented with nutrients ($NO_3^-$-N = 4.2 ± 0.2 mg $L^{-1}$, $PO_4^{3-}$-P = 0.356 ± 0.02 mg $L^{-1}$, $SiO_2$ = 10.9 ± 2.9 mg $L^{-1}$, pH = 7.1 ± 0.2, conductivity = 368 ± 5 µS $cm^{-1}$, hydraulic residence time in RAPB = 3.23 h). The inside of the RAPB was illuminated by two fluorescent lamps, resulting in a photosynthetically active radiation (PAR) irradiance level of 130 ± 20 µmol $s^{-1}$ $m^{-2}$ for air (flat quantum sensor, model LI-189, LI-COR, Inc - Lincoln - Nebraska) with light/dark periods of 16 h/8 h.

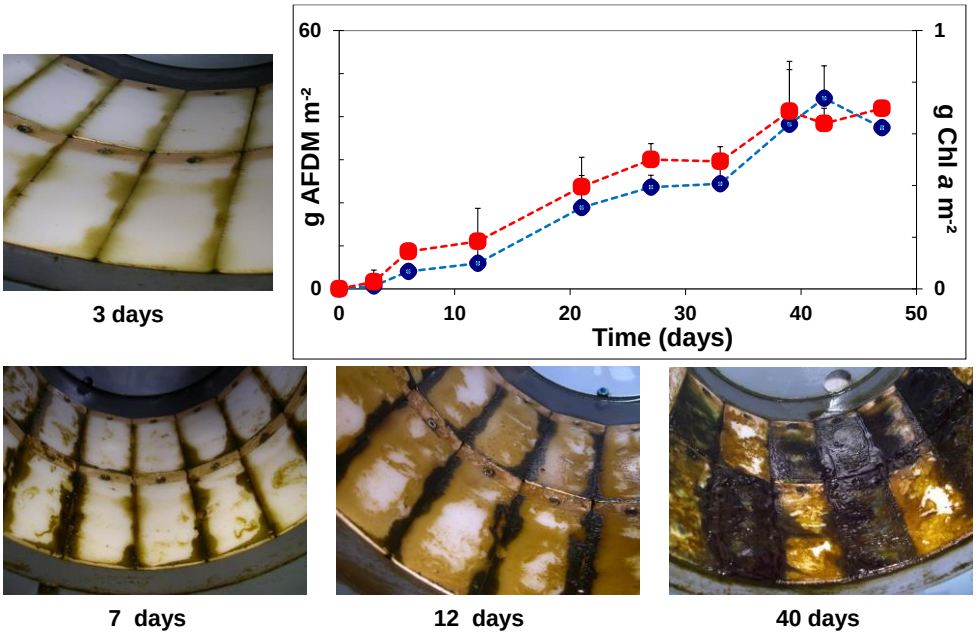


Figure 3. Temporal evolution of phototrophic biofilm biomass expressed as ash-free dry mass (AFDM, blue dots) and as chlorophyll *a* (Chl *a*, red dots) during growth in rotating annular photobioreactor. Photographic images of colonized plates at different times of growth are also shown. Partially colonized plates at day 40 correspond to newly placed plates after sampling.

In these conditions, a dry biomass production of 1.47 ± 0.37 g $m^{-2}$ $d^{-1}$ ($n$ = 6 different cultures) was obtained. At the end of the culture, the biofilm displayed a poor algal specific richness of 6 to 8 species mainly due to successional processes, although the integral biofilm and its phototrophic function were maintained (Paule et al. 2011). The chosen seeding phase limited the adhesion of microorganisms known as late colonisers and selected pioneer algal species (mainly diatoms and *Chlorophyceae*). Bacterial community structure showed a species diversity of 10 to 20 species (16S rRNA, T-RFLP). Succession was observed during the first two weeks of culture, and bacterial community strong stabilised from 3 weeks to 7 weeks of culture (Paule et al. 2011).

In our RAPB, the non-emergence of new microorganisms throughout the experiment may have caused competition even in the first step of colonisation. In microcosm studies, continuous seeding processes allows reproduction of natural conditions but can interact with the disturbance being studied. Thus, by using RAPB, we can control the experimental parameters and observe the trajectories of microbial community successions as a response to the presence of contaminants for instance.

## HYDRODYNAMIC BEHAVIOUR OF RAPB

A bioreactor with Taylor-Couette type flow displays different flow regimes (e.g., Couette, vortex flow, turbulent vortex flow and turbulent flow) depending on the rotational speed of the inner cylinder (Coufort et al. 2005). In the present RAPB design, the objective was to work with turbulent vortex flow with a sufficiently high spatial periodicity and rotational speed of the inner cylinder to prevent settling of microorganisms in the annular gap. This section describes the characterisation of the hydrodynamic behaviour of the flow in the annular space between the inner and outer cylinders through experimental and numerical studies performed at two rotational speeds, namely, 80 and 170 rpm. In these conditions, we define the dimensionless numbers used to characterise the flow regime as follows:

Reynolds number: $$\mathrm{Re} = \frac{\mathrm{ri} \cdot \Omega \cdot (\mathrm{ro} - \mathrm{ri})}{\upsilon} \quad (1)$$

Taylor number: $$\mathrm{Ta} = \mathrm{Re} \cdot \left[ \frac{(\mathrm{ro} - \mathrm{ri})}{\mathrm{ri}} \right]^{1/2} \quad (2)$$

where $ri$ is the inner cylinder radius (m), $ro$ is the outer cylinder radius (m), $\Omega$ is the angular speed of the inner cylinder (rad $s^{-1}$) and $\upsilon$ is the kinematic viscosity of the fluid (1.007 x $10^{-6}$ $m^2$ $s^{-1}$ for tap water at 20°C).

| | | |
|---|---|---|
| Rotational speed of 80 rpm: | Re = 17,040 | Ta = 6,970 |
| Rotational speed of 170 rpm: | Re = 36,210 | Ta = 14,810 |

Reynolds and Taylor numbers indicate a turbulent vortex flow with stacked axisymmetric toroidal vortices (Nemri et al. 2014).

The general mixing behaviour in RAPB was investigated experimentally using the pulse tracer method (10 mL of NaCl solution at 0.16 g $mL^{-1}$) to determine the residence time distribution (RTD). Tap water was supplied at a flow rate of 26 mL $min^{-1}$ in RAPB with a working volume of 5.04 L, resulting in an average residence time $\tau$ of 193.8 min. The conductivity of the fluid was recorded at the outlet for 15 h (corresponding to five times the average residence time) with a specific probe (conductivity meter 524, CRISON, SELI, probe response time of 2 s) located in an agitated cell (30 mL) positioned at the outlet valve in the absence of biofilm and without illumination in the RAPB.

RTD curves, defined as dimensionless concentration ($E(\theta)$) versus dimensionless time ($\theta$), were obtained from the outlet conductivity data:

$$E(\theta) = C_{(t)} / C_{(0)} \tag{3}$$

where $\theta$ is given by the ratio $t/\tau$; $C_{(t)}$ and $C_{(0)}$ are the conductivity at time $t$ and time 0, respectively, wherein $C_{(0)}$ results from an instantaneous mixing of the injected tracer.

The experimental RTD curves were compared with the RTD curve obtained from a mathematical model of reactor described by Sugiharto et al. (2009). Figure 4 compares the RTD curves based on the experimental data obtained under a rotational speed of 80 rpm and the predicted model simulation in one completely mixed reactor and two or three completely mixed reactors in series with the same total volume. The experimental and predicted model curves of one completely mixed reactor are similar. The experimental mean residence times were 209.9 and 220.8 min under rotational speeds of 80 and 170 rpm, respectively.

Numerical simulation was performed to evaluate the flow pattern within the annular gap and the characteristic turbulent scales through computational fluid dynamics (CFD) simulation by using the CFD software Fluent (6.2). The first step was to draw a grid and mesh the two-dimensional domain by using Fluent preprocessor Gambit®. The simulations were run as described by Coufort et al. (2005), that is, Reynolds Averaged Navier-Stokes equations were combined with $k$-$\varepsilon$ Reynolds Stress Model and 2Daxisymmetric model in the steady state.

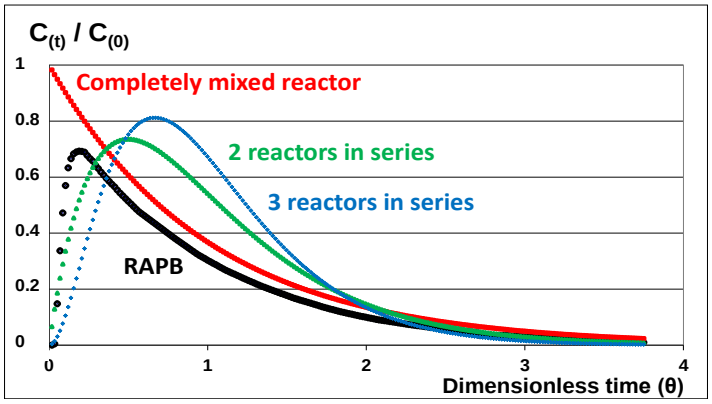


Figure 4. Comparison between experimental (black dots) and predicted (other dots) residence time distribution curves obtained under a rotational speed of 80 rpm by using rotational annular photobioreactor.

The axial average velocity profiles and the mean wall shear stress on the inner and outer cylinders (Figures 5 and 6, respectively, under the rotational speeds of 80 and 170 rpm) in the annular gap were extracted from the simulations at the scale of two vortices. The diameter of an individual vortex is approximately equal to the annular gap and thus the number of stacked vortices was 5.4 across the height (10 cm) of one plate placed on the outer cylinder in the RAPB. The presence of vortices produced a velocity gradient at a local scale on the walls of the cylinders. Consequently, wall shear stress, which is directly related to the velocity gradient, was clearly non-uniform along the plates. In the convergence zone of two vortices near the plate, the shear stress was maximal and a radial flow formed from the plate to the inner cylinder. The two vortices separated near the plate and the shear stress was minimal when the radial flow reached the plate. The magnitude of the wall shear stress along the plates increased with the rotational speed of the inner cylinder, with maximal values of 0.86 $10^{-2}$ Pa and 2.55 $10^{-2}$ Pa under the rotational speeds of 80 and 170 rpm, respectively.

Figure 7 presents the average tangential velocity profiles, which show a decrease in tangential velocity across the inner and outer cylinders, a characteristic of a turbulent vortex flow (Coufort et al. 2005). As a result, tangential velocities at the plate wall are approximately 0.3 and 0.7 m $s^{-1}$ when the rotational speeds were 80 and 170 rpm, respectively. Finally, the use of a rotational speed of the inner cylinder (80 rpm) generates a turbulent vortex flow, with a tangential velocity near the plates similar to the flow velocity in river bottom (< 0.5 m $s^{-1}$).

## INVESTIGATION OF PHOTOTROPHIC BIOFILMS

### Alachlor Ecotoxicity

The first series of ecotoxicological experiments was performed in laboratory-scale microcosms (Paule et al. 2013) to investigate the sensitivity of phototrophic biofilm communities to an herbicide in relation to the stages of phototrophic biofilm maturation (age of the phototrophic biofilms). The herbicide used was alachlor [2-chloro-*N*-(2,6-diethylphenyl)-*N*-(methoxymethyl) acetamide], which is extensively used as a pre-emergence chloroacetanilide herbicide applied to corn and soybeans. Alachlor inhibits the elongation of very long chain fatty acids in plants and algae, resulting in impaired cell development. This molecule is detected in surface waters worldwide at varying concentrations of less than 1 µg $L^{-1}$ to several tens of µg $L^{-1}$.

The phototrophic biofilms were initially cultivated in RAPB under constant operating conditions, and the results are presented in Figure 3. In RAPB, growth of biofilm was mainly driven by autogenic factors, favouring the development of simplified biofilm structures with low algal diversity. Biofilms on the plates were collected after 1.6 and 4.4 weeks of culture and then exposed to alachlor with an initial nominal concentration of 10 µg $L^{-1}$ for 15 days in microcosms. At the end of the exposure period, the effects of alachlor were monitored using a combination of the use of biomass descriptors (AFDM, Chl *a*), structural molecular fingerprinting (T-RFLP), carbon utilisation spectra (Biolog) and diatom species composition.

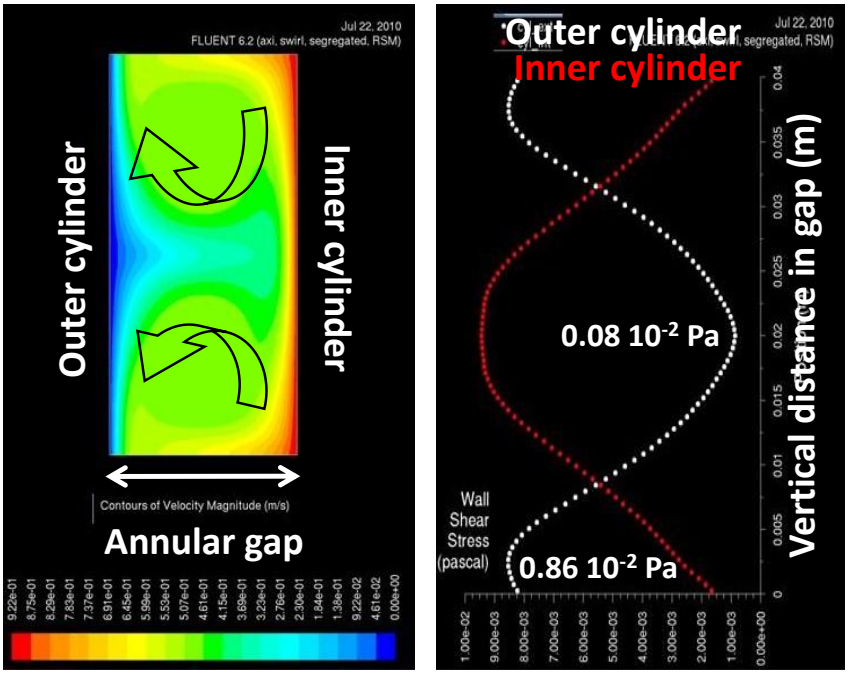


Figure 5. Contour plot of velocity magnitude field from 0 m $s^{-1}$ to 0.92 m $s^{-1}$ in the annular gap computed by computational fluid dynamics at a rotational speed of 80 rpm (left) and the corresponding wall shear stress along surface cylinders in the rotating annular photobioreactor (right).

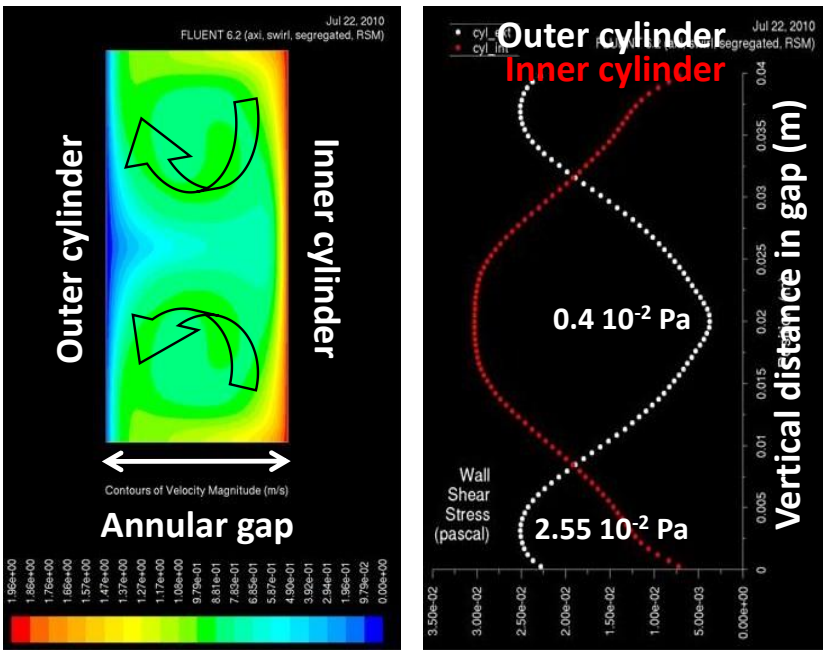


Figure 6. Contour plot of velocity magnitude field from 0 m $s^{-1}$ to 1.96 m $s^{-1}$ in the annular gap computed by computational fluid dynamics at a rotational speed of 170 rpm (left) and the corresponding wall shear stress along the surface cylinders in the rotating annular photobioreactor (right).

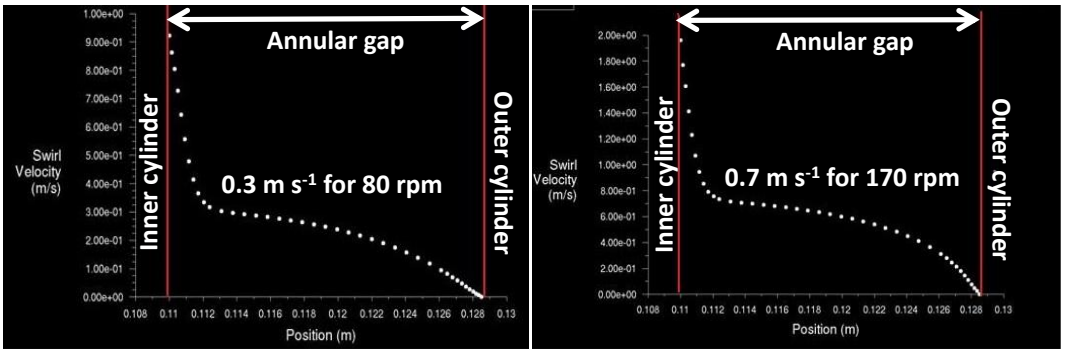


Figure 7. Profiles of tangential velocity along a line of constant height in the annular gap computed by computational fluid dynamics for rotational speeds of the inner cylinder at 80 (left) and 170 rpm (right) in the rotating annular photobioreactor.

No significant change caused by 15-day exposure to alachlor was observed in terms of bacterial and diatom community structures and carbon source utilisation profiles irrespective of development stages. Based on AFDM results, only the biomass of the "1.6-week-old biofilm" was affected, consistent with the results for growth inhibition (loss of 58% of AFDM). The three-dimensional structure of the biofilm apparently did not provide protection against the effects of alachlor. Bacterial community structure and biomass level of the "4.4-week-old biofilm" were significantly influenced by biofilm maturation processes rather than by exposure to alachlor. Diatom communities, which are largely composed of mobile and coloniser life-form populations, were not affected by alachlor. Moreover, no diatom frustules showed a significant number of deformities.

Ecologically, reduced amount of biomass (AFDM) in the early stages of growth impairs the quality of biofilm as food resource for aquatic grazers and changes the contribution of community to organic matter mineralization and element recycling. Furthermore, the absence of change in the structure and physiological states of bacterial communities as evaluated by T-RFLP and Biolog, respectively, indicated that some functions of biofilm are not affected, resulting in unperturbed overall ecosystem functioning.

In ecotoxicological experiments, taking into account the age of biofilms in the assessment of potential effects is essential. Our results showed the difficulty in distinguishing the impact of herbicide from that of other perturbations, such as incubation and operating conditions. Moreover, the intact three-dimensional structure of the biofilm apparently did not offer protection from the effects of alachlor. A multitude of effects induced by pesticides are reported in literature, and higher standards will require the use of these microbial communities as indicators. Studying phototrophic biofilms as dynamic aggregates allowed us to undertake an ecotoxicological approach integrating the concepts of ecological succession in microbial communities and the three-dimensional physical structure of the biofilm.

## Ecotoxicity of Ag Nanoparticles

Another series of ecotoxicological experiments on the effect of nanoparticles and ionic silver on phototrophic biofilms grown in RAPB under incremental inlet concentrations of silver was performed.

Given the significant increase in nanoparticle production, especially silver nanoparticles, over the past decade, the toxicity of silver in both ionic ($Ag^+$) and nanoparticle (AgNPs) forms must be extensively studied to understand their impact on natural ecosystems. AgNPs are commonly used in various industrial applications due to their specific physico-chemical properties, such as high electrical and thermal conductivity, surface-enhanced Raman scattering, chemical stability, catalytic activity and nonlinear optical behaviour. The most common applications of AgNPs includes their use as antifouling surfaces, in water purification, as aseptic food packaging, in inks, in production of renewable energies, in environmental remediation, in electronic devices and in medical field. Prior to the industrial utilisation of AgNPs, $Ag^+$was considered the most toxic form of silver in aquatic systems; however, recent investigations have demonstrated that the large surface area-to-mass ratio of small AgNPs show strong reactive interactions with extracellular and intracellular compartments of aquatic micro-organisms (e.g., Wigginton et al. 2010).

The first study allowed the characterisation of the toxic effect of $Ag^+$ and citrate coated-AgNPs in a wide concentration range (from 1 µg $L^{-1}$ to 1,000 µg $L^{-1}$) and duration of exposure (2, 5 and 14 days) on three biofilm-forming benthic microorganisms: the diatom *Nitzschia palea*, the green alga *Uronema confervicolum* and the cyanobacterium *Leptolyngbya* sp. (Gonzalez et al. 2016). These microorganisms were previously measured in RAPB experiments by using natural biofilm formed in one experimental channel. Low concentrations (1–10 µg $L^{-1}$) of $Ag^+$ significantly affect the growth of the three species, whereas the inhibitory effect of AgNPs was only observed at 1,000 µg $L^{-1}$ and only after 2 days of exposure. The inhibitory effect of both $Ag^+$ and AgNPs decreased in the course of the experiments ranging from 2 days to 14 days, and this finding can be explained by the progressive excretion of exopolysaccharides and dissolved organic carbon by the microorganisms, allowing them to alleviate the toxic effects of aqueous silver. The lower impact of AgNPs than $Ag^+$ on cells can be explained in terms of availability, internalisation, dissolved silver concentration and agglomeration of AgNPs.

A comparative study on the effect of AgNPs and ionic silver on two independent phototrophic biofilms was conducted using RAPB operated under constant conditions and during a 3-week colonisation (in the absence of silver) (Gonzalez et al. 2015). The concentration of dissolved silver (ionic or nanoparticle forms) in the inlet solution was progressively increased by stages from 0.1 µg $L^{-1}$ to 100 µg $L^{-1}$ every 4 days of exposure. In the course of the 40-day experiment, biofilm samples were collected to determine the evolution of biomass descriptors (dry mass (DM), Chl *a*), as well as photosynthetic (Phyto-Pam, Walz Mess- und Regeltechnik©) and heterotrophic enzymatic (Biolog) activities in response to addition of silver.

The presence of both AgNPs and $Ag^+$ significantly changed the biofilm structure, reducing the relative percentage of *Diatomophyceae* and *Cyanophyceae* and increasing the relative percentage of *Chlorophyceae*. Higher levels of AgNPs reduced the biomass from 8.6 ± 0.2 mgDM $cm^{-2}$ when 0–10 µg $L^{-1}$ AgNPs was added to 6.0 ± 0.1 mgDM $cm^{-2}$ when 100 µg $L^{-1}$ AgNPs was added, whereas addition of $Ag^+$ of up to 100 µg $L^{-1}$ did not exert any toxic effect

on biofilm growth. At the same time, AgNPs did not significantly affect the photosynthetic activity of the biofilm compared with $Ag^+$. These toxic effects stem from the ability of negatively charged AgNPs to move through water channels in the biofilm's EPS structure, affecting the entire ecosystem. By contrast, $Ag^+$ interacted only with the surface layers of the biofilm via adsorption on the surfaces and the EPS. Bacterial heterotrophic activity strongly decreased under an ionic silver stress of 10 μg $L^{-1}$. Moreover, heterotrophic metabolism changed at 100 μg $L^{-1}$: the biofilm used more than twice the amount of polymers under $Ag^+$ stress, whereas utilisation of amino acids and phenolic compounds decreased by nearly one order of magnitude.

Analysis of both dissolved and particulate silver allowed for the quantification of their distribution in the solution and the biofilm. Accumulation of total silver in the biofilm was proportional to the input concentration of AgNPs and $Ag^+$ in both experiments. The concentrations of accumulated silver after exposure to AgNPs were 99 μg $kgDM^{-1}$and 6.4 mg $kgDM^{-1}$ when the concentrations of AgNPs were 0.1 and 100 μg $L^{-1}$, respectively. Following the exposure to $Ag^+$, the total concentration in the biofilm ranged from 1083 mg $kgDW^{-1}$ for 0.1 μg $L^{-1}$ of $Ag^+$ to 65,800 mg $kgDW^{-1}$ for 100 μg $L^{-1}$ of $Ag^+$. These results demonstrated the exceptional capacity of the biofilm to accumulate ionic silver compared with AgNPs.

Although phototrophic biofilm can assimilate a certain amount of $Ag^+$ that is higher than that of AgNPs by an order of magnitude, the biofilm is more sensitive to AgNPs than $Ag^+$. The experiments carried out in the RAPB allow us to better understand the real effect of toxic metals, such as Ag and AgNPs, due to biofilm formation. In this sense, the batch experiments are highly affected because the microorganisms cannot produce sufficient amount of EPS to consolidate the biofilm. Overall, the phototrophic biofilm demonstrated an important capacity to accumulate silver, acting as a biological sink for this metal in natural environments and can therefore be used in bioremediation.

## Cu and Zn Interactions

Cu and Zn, which are metallic trace elements, are essential and toxic to microorganisms depending on the environmental conditions. Their environmental importance stems from their anthropogenic input, bioaccumulation potential, species-dependent toxicity and high mobility in surface waters. The circadian cycle of photosynthesis/respiration impacts the biogeochemical processes of river water with amplitude variations, which can be as large as the annual cycles (e.g. review from Nimick et al. 2011).

Interaction of Cu and Zn with phototrophic biofilm impacts the chemical and isotopic fractionation of metals at both short-term (< 2 h) and long-term (days) scale (Coutaud et al. 2014, 2017 in revision). However, the degree of metal fractionation during photosynthetic cycle of biofilm remains unknown. The present study aims to increase our knowledge on Cu and Zn cycling between a phototrophic biofilm and aqueous solution. Specifically, we focused at identifying the physico-chemical and biological mechanisms responsible for the chemical and isotopic fractionation of metals via quantifying the link between metal concentration, fluxes of sorption and excretion and related isotope fractionation.

In mature phototrophic biofilm (after 52 days of growth in RAPB), the input solution contained 1.7 and 2.9 μmol $L^{-1}$ of Cu and Zn, respectively. The output solution was regularly sampled during two continuous circadian cycles (48 h) to analyse the isotopic ratio and

concentrations of the metals. $^{66}Zn$ and $^{65}Cu$ isotope analyses in solutions and in biological matrices for the biofilm and inlet and outlet solutions were performed according to a previously described procedure (Coutaud et al. 2014, 2017 *in revision*).

The circadian cycle induced fluctuations of pH (from 6.9 to 9.8) and dissolved oxygen concentration (from 5 mg $L^{-1}$ to 20 mg $L^{-1}$) following the variation in the photosynthetic activity of the biofilm. Sorption and excretion of Cu and Zn during diel cycle of phototrophic biofilm induced significant variation in chemical and isotopic fluxes between the biofilm and aqueous solution. Diurnal variations were related to pH variation, and an increase in metal concentration in solution is related to pH reduction. The magnitude of Cu variation in solution in response to pH cycle is a factor of 50 lower than that of Zn. Diel variation in Cu in natural settings is considerably lesser than that in Zn (e.g., Pokrovsky and Shirokova 2013).

Hysteresis of metal concentration in solution over circadian cycle suggested the more important participation of active uptake than efflux in the biofilm. At night time, a net excretion of Zn and a relative excretion of Cu were observed. At daytime, the biofilm preferentially sorbed light Zn isotopes and heavy Cu isotopes from the solution with a constant isotopic fractionation $\Delta^{66}Zn_{sorbed\text{-}solution}$ of −0.1‰ ± 0.06‰ and $\Delta^{65}Cu_{sorbed\text{-}solution}$ of +0.17‰ ± 0.06‰. At night time, the biofilm excreted lighter and then heavier Zn isotopes with a $\Delta^{66}Zn_{excreted\text{-}biofilm}$ value that increases from −0.4‰ to +0.14‰ overnight. The biofilm preferentially excreted heavy isotopes with $\Delta^{65}Cu_{excreted\text{-}biofilm}$ of +0.7‰ ± 0.3‰ overnight.

The phototrophic biofilm presents a non-negligible exchange metal pool with an important potential of isotope contrasting fractionation in the diurnal scale. Our results suggest that diel photosynthetic cycles display a high concentration of dissolved Cu and Zn (a factor of 2 and 100, respectively) and isotopic variation (up to 0.73‰ and 0.76‰ for aqueous isotopic composition of Cu and Zn, respectively). We interpreted Zn and Cu diel cycles as a combination of the passive desorption of EPS-metal complexes and small active efflux at night with a passive adsorption and incorporation via an active uptake at daytime. The correlation among pH, excretion flux and metal isotopic enrichment at night time demonstrated that the metal efflux corresponded to physico-chemical desorption of Cu and Zn due to competition with $H^+$. This phenomenon should be taken into account during sample collection and during interpretation of biogeochemical and ecological features of river ecosystems.

## REFERENCES

Battin, Tom J., Louis A. Kaplan, J. Denis Newbold, and Claude M.E. Hansen. 2003. "Contributions of microbial biofilms to ecosystem processes in stream mesocosms." *Nature* 426: 439-442.

Besemer, Katharina, Gabriel Singer, Romana Limberger, Ann-Kathrin Chlup, Gerald Hochedlinger, Iris Hödl, Christian Baranyi, and Tom J. Battin. 2007. "Biophysical controls on community succession in stream biofilms." *Applied and Environmental Microbiology* 73(15): 4966-4974.

Buhmann, Matthias, Peter G. Kroth, and David Schleheck. 2012. "Photoautotrophic-heterotrophic biofilm communities: a laboratory incubator designed for growing axenic diatoms and bacteria in defined mixed-species biofilms." *Environmental Microbiology Reports* 4(1): 133-140.

Coufort, Carole, Denis Bouyer, and Alain Liné. 2005. "Flocculation related to local hydrodynamics in a Taylor-Couette reactor and in a jar." *Chemical Engineering Science* 60(8-9): 2179-2192.

Coutaud, Margot A., Merlin Méheut, Pieter Glatzel, Gleb S. Pokrovski, Jérôme Viers, Jean-Luc Rols, and Oleg S. Pokrovsky. Submitted. "Cu isotope fractionation during absorption and incorporation by a phototrophic biofilm." *Geochemica et Cosmochimica Acta* (in revision).

Coutaud, Margot A., Merlin Méheut, Jérôme Viers, Jean-Luc Rols, and Oleg S. Pokrovsky. 2014. "Zn isotope fractionation during its interaction with phototrophic biofilm." *Chemical Geology* 390: 46-60.

Flemming, Hans-Curt, and Jost Wingender. 2010. "The biofilm matrix." *Nature Reviews Microbiology* 8: 623-633.

Gonzalez, Aridane G., Lidia Fernandez-Rojo, Joséphine Leflaive, Oleg S. Pokrovsky, and Jean-Luc Rols. 2016. "Response of three biofilm-forming benthic micro-organisms to Ag nanoparticles and $Ag^{+}$: the diatom *Nitzschia palea*, the green alga *Uronema confervicolum* and the cyanobacteria *Leptolyngbya* sp." *Environmental Science and Pollution Research* 23(21): 22136-22150.

Gonzalez, Aridane G., Stéphane Mombo, Joséphine Leflaive, Alexandre Lamy, Oleg S. Pokrovsky, and Jean-Luc Rols. 2015. "Silver nanoparticles impact the phototrophic biofilm communities in a much stronger degree than the ionic silver." *Environmental Science and Pollution Research* 22 (11): 8412-8424.

Guibaud, Gilles, Eric van Hullebusch, François Bordas, and Emmanuel Joussein. 2009. "Sorption of Cd(II) and Pb(II) by exopolymeric substances (EPS) extracted from activated sludges and pure bacterial strains: Modeling of the metal/ligand ratio effect and role of the mineral fraction." *Bioresource Technology* 100: 2959-2968.

Jackson, Colin R. 2003. "Changes in community properties during microbial succession." *Oikos* 101: 444-448.

Larsen, Poul, Jeppe L. Nielsen, Morten S. Dueholm, Ronald Wetzel, Daniel Otzen, and Per Halkjaer Nielsen. 2007. "Amyloids adhesins are abundant in natural biofilms." *Environmental Microbiology* 9: 3077-3090.

Lawrence, John R., George D.W. Swerhone, and Thomas R. Neu. 2000. "A simple rotating annular reactor for replicated biofilm studies." *Journal of Microbiological Methods* 42(3): 215-224.

Lear, Gillian, Andrew Dopheide, Pierre-Yves Ancion, Kelly Roberts, Vidya Washington, Jo Smith, J., and Gillian D. Lewis. 2012. "Biofilms in freshwater: their importance for the maintenance and monitoring of freshwater health." In *Microbial Biofilms: Current Research and Applications*, edited by Gavin Lear and Gillian D. Lewis, 129-151. Caister, Caister Academic Press.

Lyautey, Emilie, Samuel Teissier, Jean-Yves Charcosset, Jean-Luc Rols, and Frédéric Garabétian. 2003. "Bacterial diversity of epilithic biofilm assemblages of an anthropised river section, assessed by DGGE analysis of 16S rDNA fragment." *Aquatic Microbial Ecology* 33: 217-224.

Lyautey, Emilie, Colin R. Jackson, Jérôme Cayrou, Jean-Luc Rols, and Frédéric Garabétian. 2005a. "Bacterial community succession in natural river biofilm assemblages." *Microbial Ecology* 50: 589-601.

Lyautey, Emilie, Bénédicte Lacoste, Loïc Ten-Hage, Jean-Luc Rols, and Frédéric Garabétian. 2005b. "Analysis of bacterial diversity in river biofilms using 16S rDNA PCR-DGGE: methodological settings and fingerprints interpretation." *Water Research* 39 (2-3): 380-388.

Nemri, Marouan, Sébastien Cazin, Sophie Charton, and Eric Climent. 2014. "Experimental investigation of mixing and axial dispersion in Taylor-Couette flow patterns." *Experiments in Fluids* 55(1769): 1-16.

Neu, Thomas R., and John R. Lawrence. 1997. "Development and structure of microbial biofilms in river water studied by confocal laser scanning microscopy." *FEMS Microbiology Ecology* 24(1): 11-25.

Nimick, David A., Christopher H. Gammons, and Stephen R. Parker. 2011. "Diel biogeochemical processes and their effect on the aqueous chemistry of streams: A review." *Chemical Geology* 283: 3–17.

Paule, Armelle, Béatrice Lauga, Loïc Ten-Hage, Jérôme Morchain, Robert Duran, Etienne Paul, and Jean-Luc Rols. 2011. "A photosynthetic rotating annular bioreactor (Taylor-Couette type flow) for phototrophic biofilm cultures." *Water Research* 45 (18): 6107-6118.

Paule, Armelle, Emilie Lyautey, Frédéric Garabétian, and Jean-Luc Rols. 2009. "Autogenic versus environmental control during development of river biofilm." *International Journal of Limnology* 45: 1-10.

Paule, Armelle, Vincent Roubeix, Béatrice Lauga, Robert Duran, François Delmas, Etienne Paul, and Jean-Luc Rols. 2013. "Changes in tolerance to herbicide toxicity throughout development stages of phototrophic biofilms." *Aquatic Toxicology* 144-145: 310-321.

Paule, Armelle, Vincent Roubeix, George D.W. Swerhone, Béatrice Lauga, Robert Duran, François Delmas, Etienne Paul, Jean-Luc Rols, and John R. Lawrence. 2016. "Comparative responses of river biofilms at the community-level to common organic solvent and herbicide exposure." *Environmental Science and Pollution Research* 23: 4282–4293.

Pokrovsky, Oleg S., and Liudmila S. Shirokova. 2013. "Diurnal variations of dissolved and colloidal organic carbon and trace metals in a boreal lake during summer bloom." *Water Research* 47: 922–932.

Sabater, Sergi, Helena Guasch, Marta Ricart, Anna Romaní, Gemma Vidal, Christina Klünder, and Mechthild Schmitt-Jansen. 2007. "Monitoring the effect of chemicals on biological communities. The biofilm as an interface." *Analytical and. Bioanalytical Chemistry* 387(4): 1425-1434.

Singer, Gabriel, Katharina Besemer, Iris Hödl, Ann-Kathrin Chlup, Gerald Hochedlinger, Peter Stadler, and Tom J. Battin. 2006. "Microcosm design and evaluation to study stream microbial biofilms." *Limnology and Oceanography-Methods* 4(11): 436-447.

Singh, Rajbir, Debarati Paul, and Rakesh K. Jain. 2006. "Biofilms: implications and bioremediation." *Trends in Microbiology* 14: 389-397.

Sugiharto, Sugiharto, Zaki Su'ud, Rizal Kurniadi, Wibisono Wibisono, and Zainal Abidin. 2009. "Radiotracer method for residence time distribution study in multiphase flow system." *Applied Radiation and Isotopes* 67(7-8): 1445-1448.

Sutherland, Ian W. 2001. "Biofilm exopolysaccharides: a strong and sticky framework." *Microbiology* 147: 3-9.

Wigginton, Nicholas S., Alexandre de Titta, Flavio Piccapietra, Jan Dobias, Victor J. Nesatyy, Marc J.F. Suter, and Rizlan Bernier-Latmani. 2010. "Binding of silver nanoparticles to

bacterial proteins depends on surface modifications and inhibits enzymatic activity." *Environmental Science & Technology* 44: 2163–2168.